Vertical Displacements Induced by Quasi-Stationary Waves in the Southern Hemisphere Stratosphere during Spring

M. MOUSTAOUI

Scripps Institution of Oceanography, University of California, San Diego, La Jolla, California

H. TEITELBAUM

Laboratoire de Meteorologie Dynamique, Ecole Normale Superieure, Paris, France

F. P. J. VALERO

Scripps Institution of Oceanography, University of California, San Diego, La Jolla, California

(Manuscript received 5 August 2002, in final form 4 February 2003)

ABSTRACT

Vertical displacements induced by the quasi-stationary wave with wavenumber 1 (QSW1) in the Southern Hemisphere stratosphere during spring are studied. The displacement exhibits two amplitude maxima located in the upper and lower stratosphere with a phase change of 180° between the two regions. Ozone mixing ratio and temperature wave signatures are explained by the wave-induced displacement in the presence of mean vertical gradients. The QSW1 induces radiative diabatic forcing in the upper stratosphere that results in a cross-isentropic ozone transport. Correlation between vertical displacement at different levels and total ozone indicates that total ozone is directly connected to the displacement in the lower stratosphere. The displacement extends to the tropopause and results in a correlation between total ozone and the tropopause height, but with smaller values. Relative deviation between reconstructed potential vorticity (PV) by using a high-resolution model and PV from observations indicates the existence of a preferred region for wave breaking and high–low-latitude air exchange, in close connection with the upward displacement and the local background flow induced by the QSW1.

1. Introduction

Stratospheric planetary waves with low zonal wavenumbers have been the subject of intensive research in many previous investigations. Statistical studies using monthly mean observations indicate that a stratospheric quasi-stationary planetary wave with the zonal wavenumber 1 (QSW1) is more intense during winter in the Northern Hemisphere, while in the Southern Hemisphere its greatest amplitude is observed during spring (Geller and Wu 1987). Some behaviors of the QSW1 in the Southern Hemisphere have been derived from multiyear observations (Randel 1988; Quintanar and Mechoso 1995; Wirth 1991). It is found that this wave is by far the dominant component of the geopotential height field in the troposphere and stratosphere of the Southern Hemisphere during spring. The amplitude of the QSW1 is largest at high latitudes (40°–70°S), with a maximum found around 10 hPa in the middle stratosphere.

Many previous studies have shown that total ozone is highly correlated with temperature and the isentropic height in the lower stratosphere (Wirth 1993; Salby and Callaghan 1993; Teitelbaum et al. 1998). Total ozone has also been found to be correlated with the tropopause height (Hoinka et al. 1996; Steinbrecht et al. 1998; Schubert and Munteanu 1988). As noted in Hoinka et al. (1996), the underlying physics connecting total ozone and tropopause height are not clear. Steinbrecht et al. (1998) attributed this correlation to photochemical ozone loss as air is shifted upward at upper levels above a rising tropopause. However, since ozone responds negatively to temperature changes under photochemical processes (Hartmann and Garcia 1979), ozone is expected to increase when air is shifted upward as the temperature decreases.

As discussed in this paper, we found that the vertical displacement of isentropes induced by the QSW1 in the stratosphere exhibits two amplitude maxima, located in the upper and lower stratosphere above and below the geopotential wave amplitude maximum, with a phase

Corresponding author address: Mohamed Moustaoui, Center for Atmospheric Sciences, Scripps Institution of Oceanography, UCSD, 9500 Gilman Drive, MC 0242, La Jolla, CA 92093-0242.
E-mail: mmoust@nuvolo.ucsd.edu

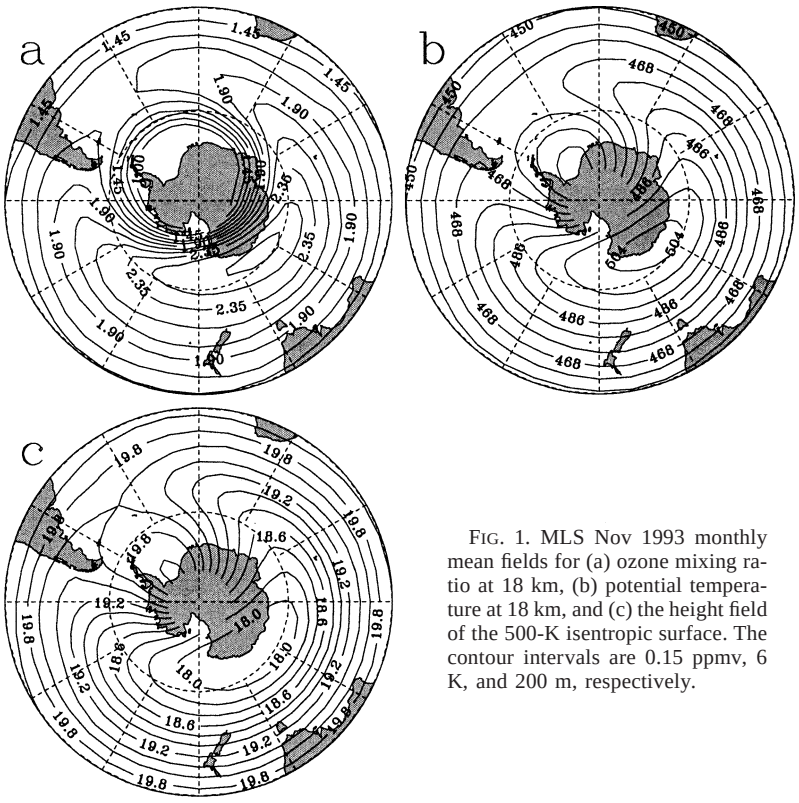

FIG. 1. MLS Nov 1993 monthly mean fields for (a) ozone mixing ratio at 18 km, (b) potential temperature at 18 km, and (c) the height field of the 500-K isentropic surface. The contour intervals are 0.15 ppmv, 6 K, and 200 m, respectively.

change of 180°- between the two regions. The impact of the wave-induced vertical displacement on ozone is studied, and contributions of the displacement at the tropopause in the lower and upper stratosphere to total ozone are discussed. Finally, we will show that the background flow induced by the QSW1 causes wave breaking and high–low-latitude air exchange to occur preferably in regions over South America.

Section 2 analyzes the role of the vertical displacement induced by the QSW1 in potential temperature and ozone mixing ratio fields observed in the lower and upper stratosphere during November 1993. In section 3, relationships between various dynamical fields induced by the wave are examined. Contributions of the vertical displacements at the tropopause in the lower and upper stratosphere to total ozone are discussed in section 4. The role of the local background flow induced by the QSW1 in the existence of a preferred region for wave breaking and high–low-latitude air mixing is shown in section 5. Finally, the results are summarized in section 6.

2. QSW1 in ozone and temperature during November 1993

The ozone and temperature data used in this section are obtained from measurements made by the Microwave Limb Sounder (MLS) instrument mounted on board the *Upper Atmosphere Research Satellite* (*UARS*; Barath et al. 1993). These data are described in many previous studies (i.e., Fishbein et al. 1996; Foirdevaux et al. 1996; Ricaud et al. 1996). The data are averaged over the period 25 October–24 November 1993 (referred to as the November mean). This period is chosen because the MLS instrument was viewing southward.

a. The lower stratosphere

Figures 1a and 1b show the November mean ozone mixing ratio and potential temperature fields at 18 km. The major features present in these fields are the ozone hole, characterized by low ozone content and associated with low temperature, and a dominance of a QSW1 in the zonal dependence. The low ozone content is primarily due to the chemical depletion that takes place during spring. The QSW1 in ozone and potential temperature are positively correlated, with higher ozone and temperature values over the lower-right quadrant and lower values over the upper-left quadrant. Figure 1c shows the November mean height field on the 500-K isentropic surface. The zonal variations are dominated by the QSW1 and are negatively correlated with ozone and temperature. The 500-K isentrope experiences an upward displacement relative to its zonal mean height over the upper-left quadrant and a downward displacement over the lower-right quadrant. Both zonal mean ozone and potential temperature increase with height in the lower stratosphere. As a consequence, at a given

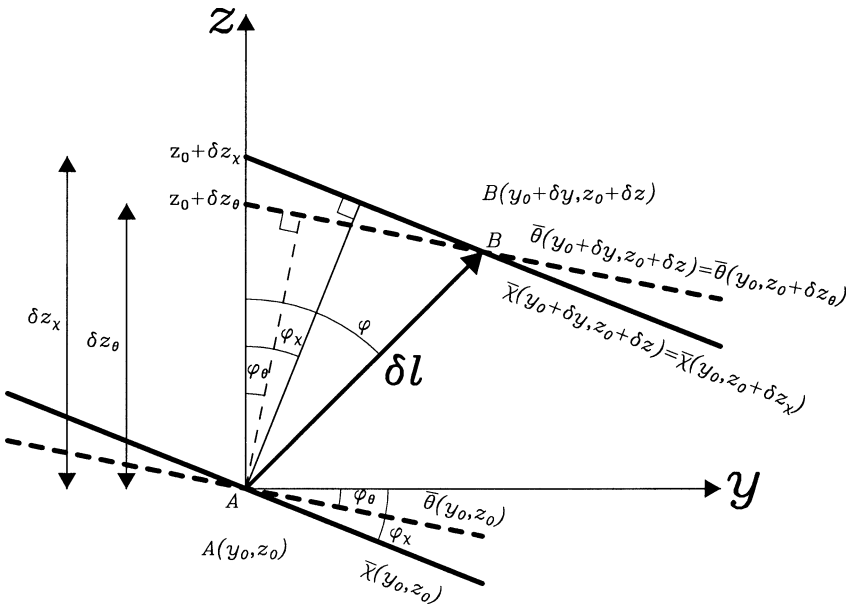

FIG. 2. Representation of a parcel displacement δl (thick arrow) induced by a wave in the presence of both horizontal and vertical gradients of ozone and potential temperature, where $A(y_0, z_0)$ and $B(y_0 + \delta y, z_0 + \delta z)$ are the initial and final parcel positions; $\overline{\chi}$ (solid thick line) and $\overline{\theta}$ (dashed thick line) are the basic ozone and potential temperature surfaces, and φ_χ and φ_θ their tilts; φ is the parcel displacement slope; and δz_χ and δz_θ are the traces on the axis $y = y_0$ of ozone and potential temperature surfaces at the final position.

height level, air shifted upward brings lower values of ozone mixing ratio and potential temperature, while air shifted downward brings higher values. This process induces perturbations in ozone and potential temperature fields that are positively correlated, as seen in Figs. 1a and 1b, while both of these fields are negatively correlated with the isentropic height (Fig. 1c).

Relationships between ozone mixing ratio and potential temperature perturbations induced by a wave can be derived. Starting from a basic state, Fig. 2, a schematic, presents a displacement of an air parcel induced by a wave from $A(y_0, z_0)$ to $B(y_0 + \delta y, z_0 + \delta z)$, in the presence of both horizontal and vertical zonal mean gradients of ozone mixing ratio and potential temperature. The mean gradients are represented by the slopes φ_χ and φ_θ of mean ozone mixing ratio ($\overline{\chi}$) and potential temperature ($\overline{\theta}$) isosurfaces, respectively.

At the final position, the parcel induces a perturbation in ozone and potential temperature that is the difference between the air parcel properties and the surrounding environment. Assuming that ozone mixing ratio and potential temperature are conserved during the transport, the induced perturbation can be expressed as the difference in the basic state properties between the initial and final positions of the parcel, given by

$$\theta' = \overline{\theta}(y_0, z_0) - \overline{\theta}(y_0 + \delta y, z_0 + \delta z) = \overline{\theta}(y_0, z_0) - \overline{\theta}(y_0, z_0 + \delta z_\theta) = -\frac{\partial \overline{\theta}}{\partial z}\delta z_\theta, \quad (1)$$

$$\chi' = \overline{\chi}(y_0, z_0) - \overline{\chi}(y_0 + \delta y, z_0 + \delta z) = \overline{\chi}(y_0, z_0) - \overline{\chi}(y_0, z_0 + \delta z_\chi) = -\frac{\partial \overline{\chi}}{\partial z}\delta z_\chi, \quad (2)$$

where δz_χ and δz_θ are, respectively, the traces on the vertical axis $y = y_0$ of the basic ozone mixing ratio and potential temperature isosurfaces at the parcel's final position (see Fig. 2). From the above relations, the following relation can be derived:

$$\chi' = \theta' \frac{\dfrac{\partial \overline{\chi}}{\partial z}}{\dfrac{\partial \overline{\theta}}{\partial z}} \frac{\delta z_\chi}{\delta z_\theta}. \quad (3)$$

This relation can be expressed as a function of the basic ozone and potential temperature surface tilts and the slope of the parcel displacement:

$$\chi' = \theta' \frac{\dfrac{\partial \overline{\chi}}{\partial z}}{\dfrac{\partial \overline{\theta}}{\partial z}} \frac{\cos(\varphi_\theta)\cos(\varphi - \varphi_\chi)}{\cos(\varphi_\chi)\cos(\varphi - \varphi_\theta)}. \quad (4)$$

Equation (4) shows the relationship between ozone-mixing-ratio and potential temperature perturbations in the presence of both vertical and horizontal mean gradients. If the mean ozone and potential temperature surfaces present similar tilts, or if these surfaces are nearly

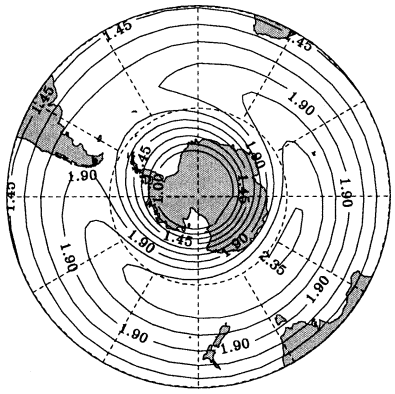

FIG. 3. Nov 1993 monthly mean ozone mixing ratio field at 18 km, reconstructed from mean vertical gradients and potential temperature perturbations (see text). The contour interval is 0.15 ppmv.

horizontal (which is the case when vertical mean gradients dominate), (4) becomes

$$\chi' = \theta' \frac{\dfrac{\partial \overline{\chi}}{\partial z}}{\dfrac{\partial \overline{\theta}}{\partial z}}. \tag{5}$$

We then remove the ozone perturbations relative to the zonal mean from the observed field shown in Fig. 1a, calculate, by using relation (5), ozone perturbations from those of potential temperature and the mean vertical gradients, and then, add them to the zonal mean ozone. The ozone-mixing-ratio field reconstructed by this method is shown in Fig. 3. This field resembles the observations, with a well-reconstructed ozone phase. Differences exist in the amplitude that are due to the chemical depletion that takes place within the ozone hole, which cannot be explained by vertical displacement, and also to horizontal contributions that are not included. These differences, however, are small, indicating that the horizontal contributions play a small role. During the period considered, the mean ozone field was dominated by the vertical gradients in the lower stratosphere (Fig. 11a).

b. The upper stratosphere

Figures 4a and 4b show the November mean ozone mixing ratio and potential temperature fields at 41 km. The QSW1 signature dominates both fields, with ozone being in opposition of phase with potential temperature. The low ozone content present in Fig. 4a is not due to the chemical depletion. The polar vortex is weak in the upper stratosphere during November (Mechoso 1990). Furthermore, the temperature field shows its highest values over the low-ozone region. These values are by far higher than the threshold value for polar stratospheric cloud (PSC) formation, which is a primary requirement for ozone chemical depletion. Comparison of the po-

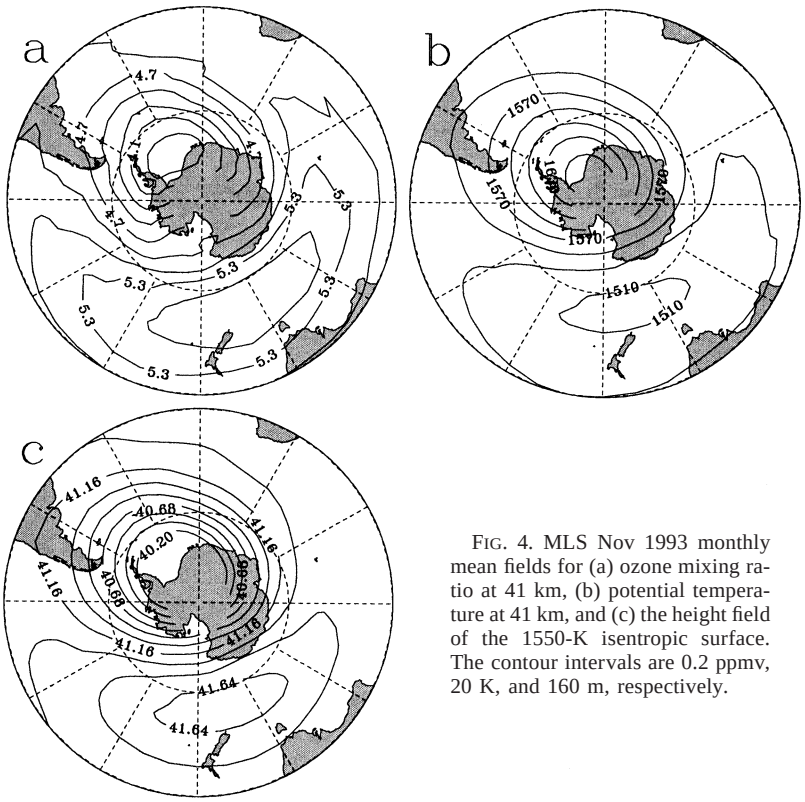

FIG. 4. MLS Nov 1993 monthly mean fields for (a) ozone mixing ratio at 41 km, (b) potential temperature at 41 km, and (c) the height field of the 1550-K isentropic surface. The contour intervals are 0.2 ppmv, 20 K, and 160 m, respectively.

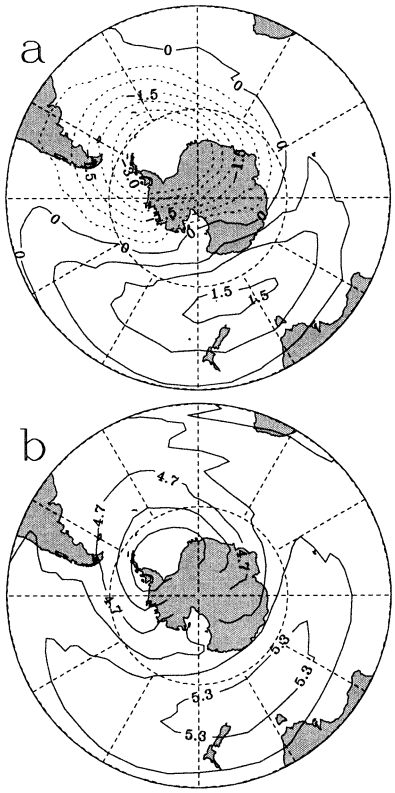

FIG. 5. Nov 1993 monthly mean (a) diabatic heating field at 41 km, computed by using the NCAR CRM and MLS data and (b) the ozone mixing ratio field at 1550 K. The contour intervals are 0.5 K day^{-1} and 2 ppmv, respectively.

tential temperature field between the upper and lower stratosphere (Figs. 4b and 1b, respectively) exhibits a phase difference of about 180°. This behavior will be discussed in the next section. Figure 4c shows the November mean height field of the 1550-K isentropic surface. It shows higher potential temperature values in the region where the isentrope experiences downward displacement and lower values in the region where it bows up, indicating the role of the vertical displacements.

Following Hartmann and Garcia (1979), the level considered is located in the transition region between dynamically and photochemically controlled regions. Then, both processes are expected to play a role in the ozone field. Ozone responds negatively to temperature under a photochemical process. However, negative ozone–temperature correlation is not necessarily by itself a signature of a photochemical effect. In the upper stratosphere, the mean ozone profile decreases with height. Vertical displacements may explain the phase difference between ozone and temperature in the upper stratosphere. However, vertical displacement alone cannot explain the ozone field shown in Fig. 4a. A field reconstructed by taking into account only the vertical displacement shows smaller amplitude.

Radiative processes are important in the upper stratosphere. They usually act to damp out temperature perturbations away from an equilibrium profile (Fels 1982). Figure 5a shows the November mean diabatic forcing field computed by using the Column Radiation Model (CRM) of the National Center for Atmospheric Research (NCAR) Community Climate Model Version 3 (CCM3; Kiehl 1998), together with the temperature and ozone fields observed by the MLS during the same period. The QSW1 signature dominates this field. The diabatic forcing is 180° out of phase relative to the temperature (Fig. 4b). A downward displacement induced by the QSW1 produces an adiabatic heating, while an upward displacement induces an adiabatic cooling. The adiabatic forcing pushes the atmosphere away from its equilibrium state. Then, the radiative processes tend to respond to this change by removing the forcing in order to restore the equilibrium state. As a result, a diabatic forcing takes place and opposes that induced adiabatically by the vertical motion. The diabatic processes result in a cross-isentropic ozone transport. Since the mean ozone vertical profile in the upper stratosphere decreases with height, this transport brings a high ozone value to an isentrope in the diabatic heating region and a low ozone value in the diabatic cooling region. As a consequence, the ozone field, when plotted on an isentropic surface, exhibits a QSW1 signature that is in phase with the diabatic heating. This behavior is clearly depicted in Fig. 5b, in which the ozone distribution on the 1550-K isentropic surface is shown.

3. Relationships between wave pattern in different atmospheric parameters

a. 1993 wave behavior using UARS

Figure 6a shows a latitude–height cross section for the QSW1 amplitude present in the temperature field. It shows high values at high latitudes. Unlike the geopotential wave amplitude (Fig. 6c), the temperature wave exhibits two localized amplitude maxima located in the lower and upper stratosphere. Figure 6b shows a latitude–height cross section for the QSW1 amplitude present in the vertical displacement field. The vertical displacement denotes the deviation of the height of an isentrope relative to its zonal mean level. It shows a pattern that resembles the temperature, with two amplitude maxima present in the lower and upper stratosphere, indicating the role of the wave-induced vertical displacement in the observed temperature.

Figure 7 shows longitude–height cross sections at 65°S for the QSW1 perturbation present in the temperature, vertical displacement, and vorticity fields. The vorticity was derived from the geopotential by assuming the geostrophic approximation. Both temperature and displacement exhibit a phase difference of 180° between the lower and upper stratosphere (Figs. 7a, b). Also, the temperature is in opposition of phase relative to the displacement at both levels. The vorticity perturbation (Fig. 7c) shows a single maximum located around 26

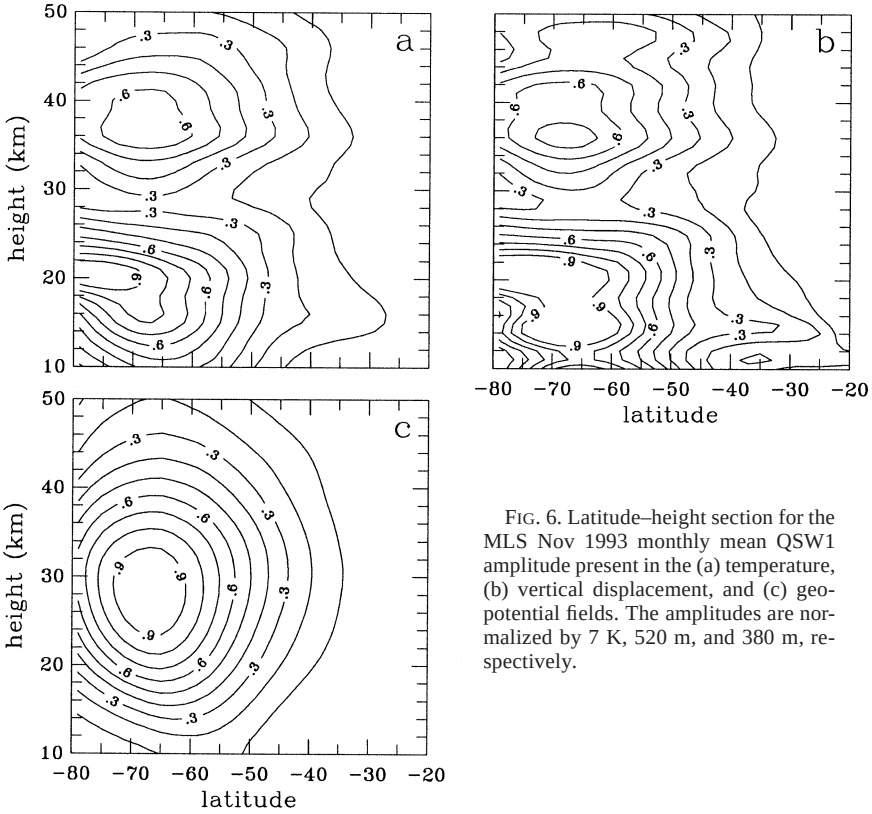

FIG. 6. Latitude–height section for the MLS Nov 1993 monthly mean QSW1 amplitude present in the (a) temperature, (b) vertical displacement, and (c) geopotential fields. The amplitudes are normalized by 7 K, 520 m, and 380 m, respectively.

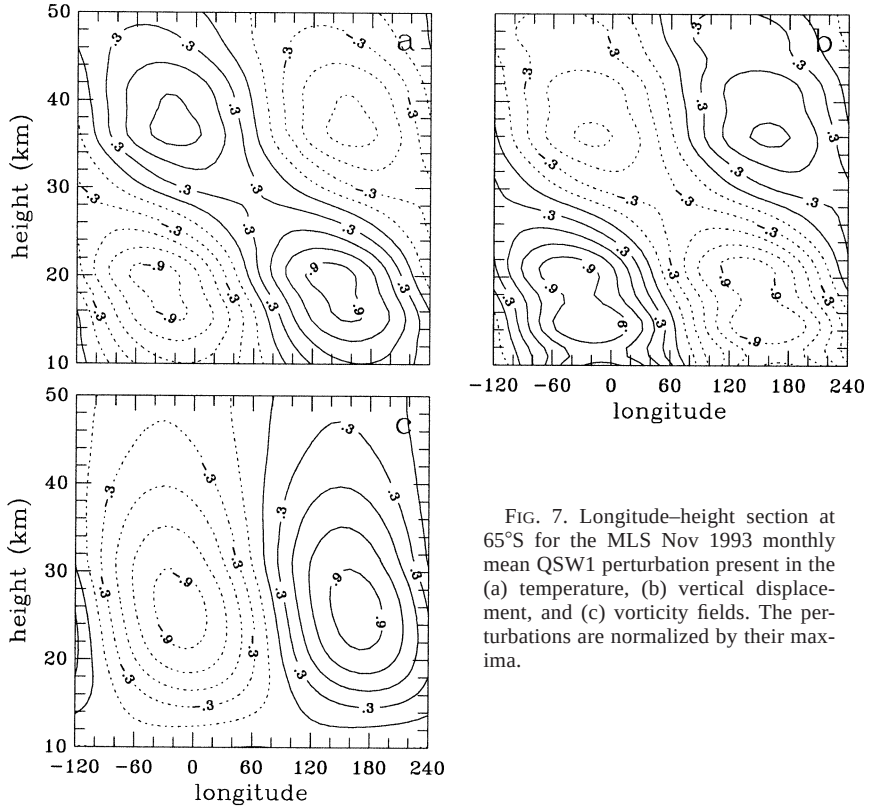

FIG. 7. Longitude–height section at 65°S for the MLS Nov 1993 monthly mean QSW1 perturbation present in the (a) temperature, (b) vertical displacement, and (c) vorticity fields. The perturbations are normalized by their maxima.

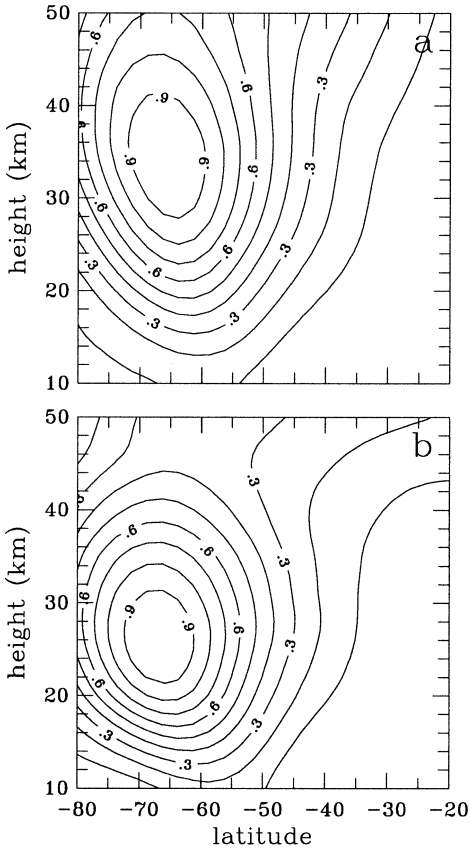

FIG. 8. Latitude–height section for the QSW1 amplitude present in geopotential fields obtained from 10-yr UKMO data for (a) Oct and (b) Nov. The amplitude is normalized by 414 m.

km. Comparison between the above fields shows that isentropes bow toward the cyclonic center (30°W) and away from the anticyclonic center (150°E). These relationships are consistent with those found in previous theoretical investigations (Hoskins et al. 1985; Bishop and Thorpe 1994) in which the effect of cyclonic and anticyclonic anomalies at the tropopause was studied.

b. Wave and mean wind relationship

The observed wave behavior during 1993 is a climatological feature and not just a peculiarity of that year. The wave present in a 10-yr period (not shown) shows similar patterns. During spring, the temperature increase over polar regions in the Southern Hemisphere produces easterly winds that appear first in the upper stratosphere and then gradually spread down to low levels (Mechoso et al. 1989). The zonal-mean-wind variation affects the wave propagation and causes the level at which these patterns take place to be shifted down with time (Fig. 8). Simple linear simulations can qualitatively reproduce this change. The model used is similar to that in Matsuno (1970). It is based on the linearized quasigeostrophic potential vorticity equation in spherical coordinates, which takes the form

$$\left(\frac{\partial}{\partial t} + \frac{\overline{u}}{a\cos\varphi}\frac{\partial}{\partial\lambda}\right)q' + \frac{\overline{q}_\varphi}{fa^2\cos\varphi}\frac{\partial\phi'}{\partial\lambda} = 0, \quad (6)$$

where

$$q' = \frac{1}{fa^2}\left[\frac{\phi'_{\lambda\lambda}}{\cos^2\varphi} + \frac{f^2}{\cos\varphi}\left(\frac{\cos\varphi}{f^2}\phi'_\varphi\right)_\varphi + \frac{f^2a^2}{\rho_0}\left(\frac{\rho_0\phi'_z}{N^2}\right)_z\right] \quad (7)$$

and

$$\overline{q}_\varphi = 2\Omega\cos\varphi - \left[\frac{(\overline{u}\cos\varphi)_\varphi}{a\cos\varphi}\right]_\varphi - \frac{a}{\rho_0}\left(\frac{\rho_0 f^2}{N^2}\overline{u}_z\right)_z, \quad (8)$$

where q' and ϕ' are the potential vorticity and geopotential perturbations, and $\overline{u}$ and $\overline{q_\varphi}$ are zonal mean wind and mean meridional potential vorticity gradient, respectively. Since we are concerned with the QSW1, the time derivative is removed from (6), and the zonal wavenumber 1 is imposed for the zonal dependence. Equations (6) and (7) are then combined to obtain a two-dimensional (latitude–height) elliptical partial differential equation for the geopotential perturbation. This equation is solved numerically for October and November between 10 and 52 km and for latitudes between 84° and 16°S. The finite-difference grid used has increments of 4° in latitude and 2 km in the vertical direction. A small dissipation is introduced to avoid critical lines where the mean wind equals zero. For each month, a 10-yr zonal-mean-wind field is obtained from the U.K. Met Office (UKMO) data. At the bottom boundary, the geopotential wave obtained from the UKMO data at 10 km is prescribed, while at the upper boundary a 5-km-deep sponge layer is imposed. The simulated wave amplitude (Fig. 9) qualitatively resembles the observations (Fig. 8). Even in linear considerations, the level of the amplitude maximum shows a decrease between October and November. However, the QSW1 and the mean flow do not evolve independently of each other. As the wave propagates upward, it interacts with the mean flow. This interaction is particularly important when the wave reaches its critical level, where the zonal mean wind is equal to zero. Near this level, the wave is absorbed by the mean flow, and the resulting interaction causes the critical level to move downward.

4. Impact of vertical displacements on total ozone

Figure 10 shows a November climatological latitude–height cross section for correlation between total ozone and the vertical displacement of isentropes at different levels calculated from the National Centers for Environmental Prediction (NCEP)–NCAR reanalysis. Ozone data are obtained from measurements made by the Total Ozone Mapping Spectrometer (TOMS) instrument mounted on board the *Nimbus-7, Meteor-3,* and *Earth Probe* satellites. The period chosen extends from 1980 to 1999, except for 1993, 1994, and 1995, when the TOMS data were not available. The QSW1 is by far the

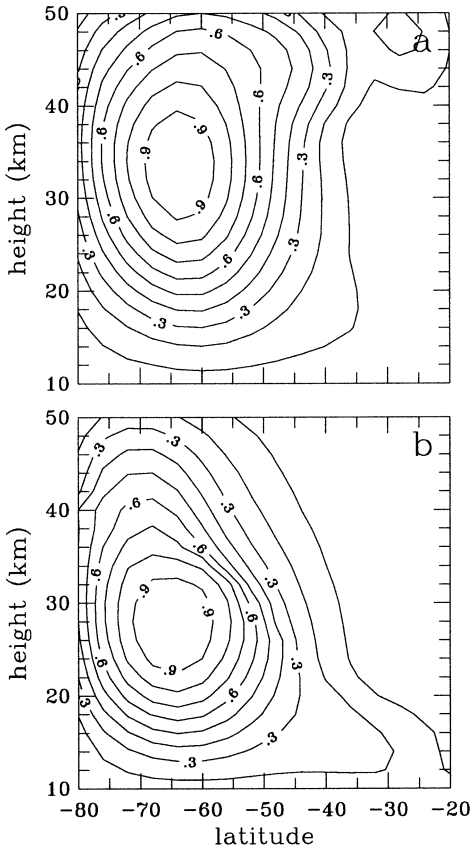

FIG. 9. Latitude–height section for the QSW1 amplitude present in a simulated geopotential field for (a) Oct and (b) Nov.

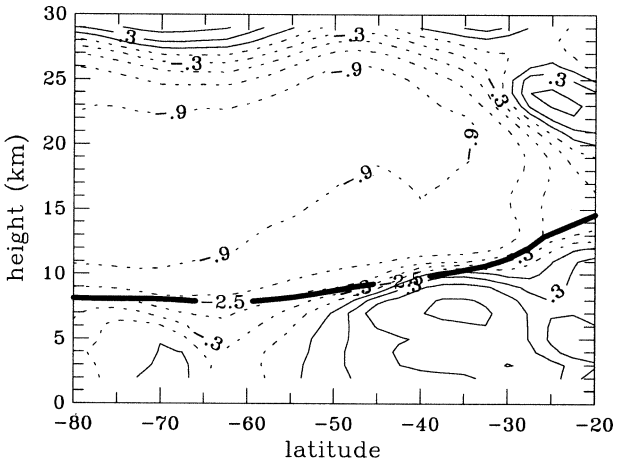

FIG. 10. Latitude–height section for the climatological correlation between total ozone and the vertical displacement at different levels. The contour interval is 0.2. The thick line is the potential vorticity contour, −2.5 PVU, that represents the tropopause (1 PVU = 10^{-6} m^2 K kg^{-1} s^{-1}).

dominant component in the zonal dependence of the ozone and the displacement fields. The correlation at the tropopause (the tick line) is about 0.5, which is similar to that found in Hoinka et al. (1996). However, the strongest correlation is found in the lower stratosphere, where the absolute value of correlation is larger than 0.9, with more than 0.99 significance. This indicates that, although total ozone is correlated with tropopause height, it appears to be closely connected with the vertical displacement induced in the lower stratosphere. In this region, the local ozone density is higher and most of the contribution to total ozone is found. Thus, total ozone is more sensitive to the expansion and compression effects produced by the vertical displacement in the lower stratosphere. However, since the vertical displacement extends to the tropopause, total ozone is also correlated with tropopause height.

NCEP reanalysis data are not available at upper-stratospheric levels. To find an effect of the vertical displacements at these levels, we have used the MLS data presented in the previous sections. Figures 11a and 11b show cross sections for the zonal mean ozone mixing ratio and the correlation between the vertical displacement and the ozone mixing ratio at each level. For levels below 26 and above 38 km, where the mean ozone is dominated by vertical gradients, the correlation is higher than 0.9. Between 26 and 38 km, the mean ozone shows high horizontal gradients and a relatively small correlation. The positive correlation in the upper stratosphere is due to the change in the vertical gradient sign and, even more so, to the photochemical ozone response to the temperature change induced by the vertical displacement. Figure 11c shows a cross section for correlation between the vertical displacement at different levels and total ozone calculated from the MLS. It shows high correlation with opposite signs in the lower and upper stratosphere. The level at which the correlation changes sign coincides with the level at which there is a phase variation in the displacement (Fig. 7b). The high correlation found at upper-stratospheric levels reflects this phase variation and is not likely to be due to the ozone contribution at these levels. For instance, at 60°S, the correlation with total ozone is about 0.9 at 34 km, while that with the ozone mixing ratio is less than 0.3.

The correlation we found in the lower stratosphere is comparable with the results of Salby and Callaghan (1993), who found a correlation of 0.88 between total ozone and the pressure field at 375 K during October in the Southern Hemisphere. They attributed the high correlation to the smaller role of the horizontal transport in the Southern Hemisphere. The contributions of the horizontal and vertical transports vary with the hemisphere and the season. Equal contributions have been found during winter in the Northern Hemisphere (Kurzeja 1984) and during summer in the Southern Hemisphere (Schoeberl and Krueger 1983). Our results contrast with the Steinbrecht et al. (1998) hypothesis, who conclude that if the tropopause were shifted up, then lower-stratospheric ozone mixing ratio would be moved away, and excess ozone shifted into higher levels would be destroyed photochemically, resulting in a decrease

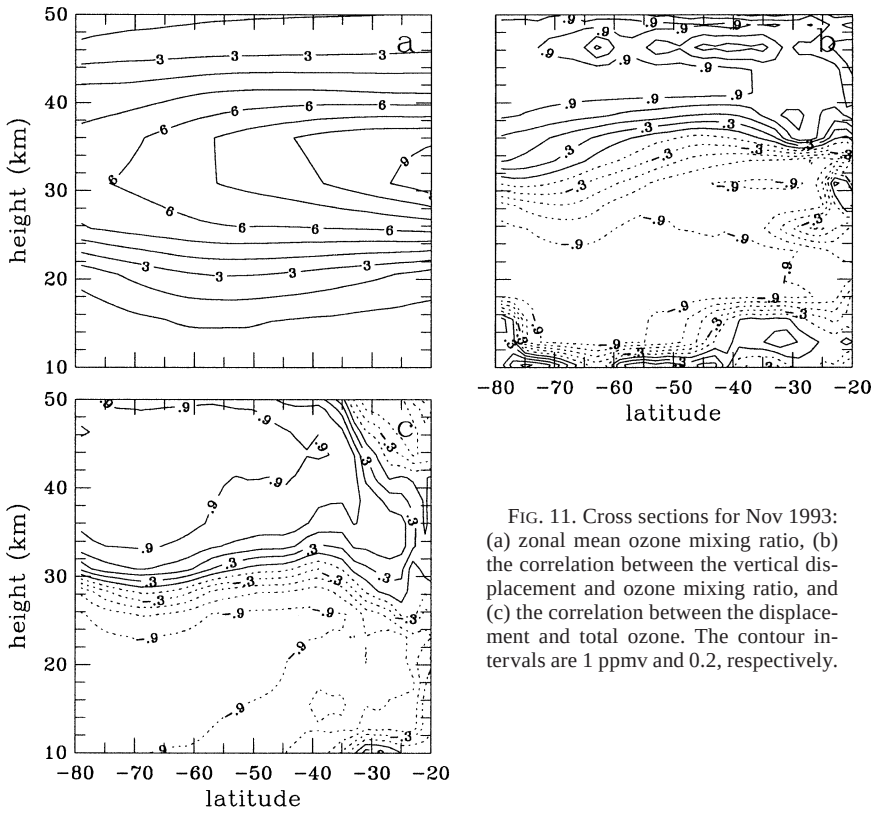

FIG. 11. Cross sections for Nov 1993: (a) zonal mean ozone mixing ratio, (b) the correlation between the vertical displacement and ozone mixing ratio, and (c) the correlation between the displacement and total ozone. The contour intervals are 1 ppmv and 0.2, respectively.

of total ozone. However, the vertical displacement field presented in Fig. 7b indicates that above the region where the lower stratosphere is shifted up, a downward displacement is found. Furthermore, if the total-ozone decrease above the rising tropopause was produced by photochemical ozone loss as the ozone profile is shifted up at upper levels, then ozone and vertical shifting would be strongly and negatively correlated at these levels. However, the correlation field presented in Fig. 11c shows positive values above 30 km. As a consequence, photochemical destruction above the tropopause rising region is not required for total ozone decrease. An upward motion in the lower stratosphere may produce a dynamical decrease in total ozone. The upshift at upper-stratospheric levels may actually produce a photochemical ozone increase as air cools, which results in a positive correlation between the displacement and the ozone mixing ratio, as seen in Fig. 11b at these levels.

5. Connection between the QSW1 and a preferred region for high–low-latitude exchange

Monthly mean averaging removes the shorter-scale dynamical processes. Many previous studies have shown the importance of wave breaking in the erosion process of the polar vortex (i.e., McIntyre and Palmer 1983; Juckes and McIntyre 1987). Observations and high-resolution modeling studies have indicated that the erosion is accompanied by development of filaments that irreversibly transport air from the vortex edge toward the equator (i.e., Waugh et al. 1994; Mariotti et al. 1997). Wave breaking appears to be one-sided, in that air expelled from the vortex edge tends to be transported toward the equator (i.e., Polvani and Plumb 1992). The one-sidedness of wave breaking was explained by across-jet asymmetry of the flow, which is, under most circumstances, such that waves break uniquely outward (Nakamura and Plumb 1994).

To find a possible connection between the QSW1 and high–low-latitude exchange, we have reconstructed potential vorticity (PV) fields at 600 K by using a high-resolution model in which the adiabatic assumption was adopted and the domain-filling technique was implemented. For each day in the 18-day period 25 October–11 November 1993, when the QSW1 amplitude was higher, the PV field is computed by initializing the model 7 days before, and the absolute deviation of the reconstructed field relative to the reanalyzed one is calculated. The relative deviation indicates the presence of either diabatic processes or filaments. Diabatic effects mix air masses across PV contours and are missed in the reconstructed fields. Filaments, however, are missed in the reanalyzed fields because of low resolution. Figure 12 shows the relative deviation field averaged over the 18-day period. It shows a wavenumber-1 structure, with higher values over regions near South America. This result indicates that these regions are preferred re-

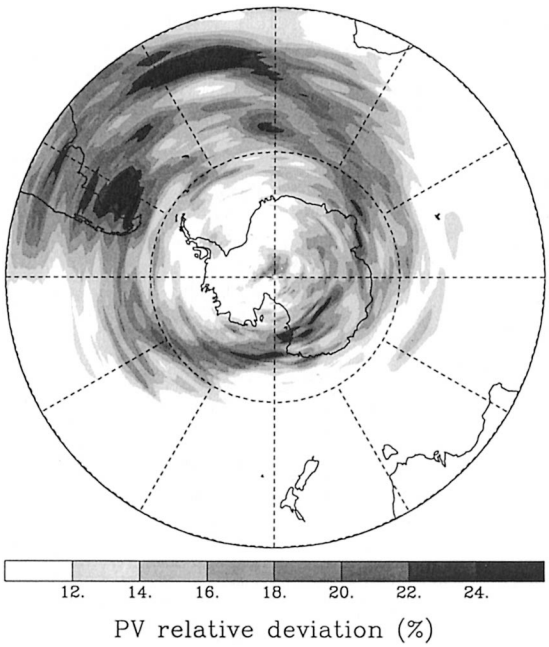

FIG. 12. Relative deviation between reconstructed and reanalyzed PV fields at 600 K, averaged over the period 24 Oct–11 Nov 1993.

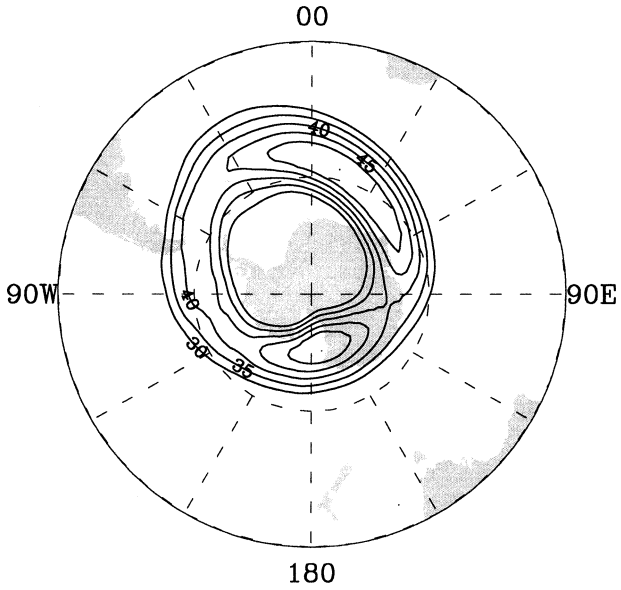

FIG. 13. The zonal wind at 600 K, averaged over the same period as in Fig. 12. The contour interval is 5 m s^{-1}.

gions for wave breaking and air mixing, in close connection with the upward displacement induced by the QSW1. The high PV gradient characterizing the vortex edge is directly responsible in the polar vortex isolation (McIntyre 1989; Juckes and McIntyre 1987). When a portion of the vortex edge experiences upward motion, it dilates (Teitelbaum et al. 1998). The dilation results in a relatively weaker PV gradient that presents less resistance to the sideways displacements across that portion of the vortex edge. The local background flow induced by the QSW1 plays an important role in the location of wave breaking. Figure 13 shows the zonal wind field at 600 K, averaged over the same period as in Fig. 12. It shows a jet with weak winds over regions near South America. The impact of zonal variations in a mean flow on wave breaking have been recently investigated (Peters and Waugh 1996; Swanson et al. 1997; Swanson 2000). It was found that wave breaking occurs in regions where the zonal mean wind is weak. The structure of the flow shown in Fig. 13 indicates that waves propagating along the jet are expected to break preferably in regions over South America, resulting in the higher relative deviation found in those regions.

6. Conclusions

The present study investigates vertical displacements induced by quasi-stationary waves in the Southern Hemisphere stratosphere during spring. The vertical displacement and temperature wave exhibit two amplitude maxima located in the upper and lower stratosphere, with a phase change of 180° between the two regions. The vertical displacement appears to play a dominant role in the temperature and ozone wave for the period considered. These wave patterns shift down with time as a consequence of mean wind change. The QSW1 indirectly induces radiative diabatic forcing in the upper stratosphere that results in a damping of temperature and a cross-isentropic ozone transport.

The correlation between vertical displacement at different levels and total ozone indicates that, although total ozone is correlated with the tropopause (0.5), it is closely connected with vertical displacements induced in the lower stratosphere, where the correlation is over 0.9. Since the contribution to total ozone is higher in the lower stratosphere, total ozone is more sensitive to density variation induced by the displacement in that region. The displacement extends to the tropopause and results in a correlation between total ozone and tropopause height, but with smaller values. In contrast with the Steinbrecht et al. (1998) hypothesis, upshift and photochemical ozone loss in upper levels above a rising tropopause are not required to explain total-ozone and tropopause-height correlation.

The mean relative deviation between reconstructed PV and PV obtained from the reanalysis exhibits a QSW1 shape with high values over the region where the wave induces upward displacements. The relative deviation indicates a statistical measure for wave breaking and a possible isentropic air mixing. It shows that isentropic air mixing is likely to occur in regions over South America where isentropes are shifted up. Upward displacement produces polar-vortex-edge dilation that decreases the PV gradient and results in relatively weaker polar-vortex-edge isolation. Furthermore, the background flow induced by the QSW1 shows weak winds

in regions over South America. Waves propagating along the vortex edge break preferably in that region. The QSW1 does not experience phase variation year after year. Then, regions located near South America are expected to be climatological preferred regions for air exchange between high and low latitudes during spring. Finally, the quasi-stationary waves with lowest wavenumbers (2, 3, . . .) seem to play a very small role in the results presented in this paper. The temperature at 18 km and 60°S indicates that the QSW1 alone explains 96% of the zonal variance for the period 25 October–24 November 1993. For the climatological fields used in Fig. 10, the variance explained by the QSW1 is more than 98%.

Acknowledgments. The authors would like to thank W. J. Randel for the UKMO data provided at the SPARC data center. The authors also thank the CCM group at NCAR for the column radiation model, and the MLS team at the British Atmospheric Data Center. The NCEP reanalysis data were obtained from the NOAA–CIRES Climate Diagnostics Center. The National Aeronautics and Space Administration ozone-processing team at the Goddard Space Flight Center provided the TOMS data. This study was supported by NASA Grant NAS5-99120 to the Scripps Institution of Oceanography, University of California, San Diego. The authors also acknowledge unknown referees for useful suggestions and comments.

REFERENCES

Barath, F. T., and Coauthors, 1993: The upper atmosphere research satellite microwave limb sounder instrument. *J. Geophys. Res.*, **98,** 10 751–10 762.

Bishop, C. H., and A. J. Thorpe, 1994: Potential vorticity and electrostatics analogy: Quasi-geostrophic theory. *Quart. J. Roy. Meteor. Soc.,* **120,** 713–731.

Fels, S. B., 1982: A parameterization of scale-dependent radiative damping in the middle atmosphere. *J. Atmos. Sci.,* **39,** 1141–1152.

Fishbein, E. F., and Coauthors, 1996: Validation of UARS Microwave Limb Sounder temperature and pressure measurements. *J. Geophys. Res.,* **101,** 9983–10 016.

Foirdevaux, L., and Coauthors, 1996: Validation of UARS MLS ozone measurements. *J. Geophys. Res.,* **101,** 10 017–10 060.

Geller, M. A., and M. F. Wu, 1987: Troposphere–stratosphere general circulation statistics. *Transport Processes in the Middle Atmosphere,* G. Visconti and R. Garcia, Eds., Reidel, 3–17.

Hartmann, D. L., and R. R. Garcia, 1979: A mechanistic model of ozone transport by planetary waves in the stratosphere. *J. Atmos. Sci.,* **36,** 350–364.

Hoinka, K. P., H. Claude, and U. Kohler, 1996: On the comparison between tropopause pressure and ozone above Central Europe. *Geophys. Res. Lett.,* **23,** 1753–1756.

Hoskins, B. J., M. E. McIntyre, and A. W. Robertson, 1985: On the use and significance of isentropic potential vorticity maps. *Quart. J. Roy. Meteor. Soc.,* **111,** 877–946.

Juckes, M. N., and M. E. McIntyre, 1987: A high resolution one-layer model of breaking planetary waves in the stratosphere. *Nature,* **328,** 590–596.

Kiehl, J. T., J. J. Hack, G. B. Bonan, B. A. Boville, D. L. Williamson, and P. J. Rasch, 1998: The National Center for Atmospheric Research Community Climate Model: CCM3. *J. Climate,* **11,** 1131–1150.

Kurzeja, J. R., 1984: Spatial variability of total ozone at high latitudes in winter. *J. Atmos. Sci.,* **41,** 695–697.

Mariotti, A., M. Moustaoui, B. Legras, and H. Teitelbaum, 1997: Comparison between vertical ozone soundings and reconstructed potential vorticity maps by contour advection with surgery. *J. Geophys. Res.,* **102,** 6131–6142.

Matsuno, T., 1970: Vertical propagation of stationary planetary waves in the winter Northern Hemisphere. *J. Atmos. Sci.,* **27,** 871–883.

McIntyre, M. E., 1989: On the antarctic ozone hole. *J. Atmos. Terr. Phys.,* **51,** 29–43.

——, and T. N. Palmer, 1983: Breaking planetary waves in the stratosphere. *Nature,* **305,** 593–600.

Mechoso, R. C., 1990: The final warming of the stratosphere. *Dynamics, Transport and Photochemistry in the Middle Atmosphere of the Southern Hemisphere,* A. O'Neill, Ed., Kluwer Academic, 55–69.

——, A. O'Neill, J. D. Farrara, V. D. Pope, and D. Pan, 1989: Interhemispheric comparison of the fall and spring circulations in the middle atmosphere. Preprints, *Third Int. Conf. on Southern Hemisphere Meteorology and Oceanography,* Buenos Aires, Argentina, Amer. Meteor. Soc., 421–428.

Nakamura, M., and R. A. Plumb, 1994: The effect of flow asymmetry on the direction of Rossby wave breaking. *J. Atmos. Sci.,* **51,** 2031–2045.

Peters, D., and D. W. Waugh, 1996: Influence of barotropic shear on the poleward advection of upper tropospheric air. *J. Atmos. Sci.,* **53,** 3013–3031.

Polvani, L. M., and R. A. Plumb, 1992: Rossby wave breaking, filamentation and secondary vortex formation: The dynamics of a perturbed vortex. *J. Atmos. Sci.,* **49,** 462–476.

Quintanar, A. I., and C. R. Mechoso, 1995: Quasi-stationary waves in the Southern Hemisphere. Part I: Observational data. *J. Climate,* **8,** 2659–2672.

Randel, W. J., 1988: Seasonal evolution of planetary waves in the Southern Hemisphere stratosphere and troposphere. *Quart. J. Roy. Meteor. Soc.,* **114,** 1385–1409.

Ricaud, P., J. Delanoe, B. J. Connor, L. Froidevaux, J. W. Waters, R. S. Harwood, L. A. Mackenzie, and G. E. Peckham, 1996: Diurnal variability of mesospheric ozone as measured by the UARS microwave limb sounder instrument: Theoretical and ground-based validations. *J. Geophys. Res.,* **101,** 10 077–10 089.

Salby, M. L., and P. F. Callaghan, 1993: Fluctuations of total ozone and their relationship to stratospheric air motions. *J. Geophys. Res.,* **98,** 2715–2727.

Schoeberl, M. R., and A. J. Krueger, 1983: Medium scale disturbances in total ozone during Southern Hemisphere summer. *Bull. Amer. Meteor. Soc.,* **64,** 1358–1365.

Schubert, S. D., and M. J. Munteanu, 1988: An analysis of tropopause pressure and total ozone correlation. *Mon. Wea. Rev.,* **116,** 569–582.

Steinbrecht, W., H. Claude, U. Koler, and K. P. Hoinka, 1998: Correlations between tropopause height and total ozone: Implications for long term changes. *J. Geophys. Res.,* **103,** 19 183–19 192.

Swanson, K. L., 2000: Stationary wave accumulation and the generation of low-frequency variability on zonally varying flows. *J. Atmos. Sci.,* **57,** 2262–2280.

——, P. J. Kushner, and I. M. Held, 1997: Dynamics of barotropic storm tracks. *J. Atmos. Sci.,* **54,** 791–810.

Teitelbaum, H., M. Moustaoui, P. F. J. van Velthoven, and H. Kelder, 1998: Decrease of total ozone at low latitudes in the Southern Hemisphere by a combination of linear and nonlinear processes. *Quart. J. Roy. Meteor. Soc.,* **124,** 2625–2644.

Waugh, D. W., and Coauthors, 1994: Transport out of the lower stratospheric Arctic vortex by Rossby wave breaking. *J. Geophys. Res.,* **99,** 1071–1088.

Wirth, V., 1991: What causes the seasonal cycle of stationary waves in the southern stratosphere? *J. Atmos. Sci.,* **48,** 1194–1200.

——, 1993: Quasi-stationary planetary waves in total ozone and their correlation with lower stratospheric temperature. *J. Geophys. Res.,* **98,** 8873–8882.